Limiting the effects of earthquakes on gravitational-wave interferometers

Sebastien Biscans and Fred Donovan
LIGO Laboratory, Massachusetts Institute of Technology, Cambridge, MA 02138, USA

Christopher Buchanan
Department of Physics and Astronomy, Louisiana State University, Baton Rouge, LA 70803-4001, USA

Eric Coughlin
Department of Computer Science, Luther College, 700 College Dr, Decorah, IA 52101, USA

Michael Coughlin
Department of Physics, Harvard University, Cambridge, MA 02138, USA

Paul Earle, Jeremy Fee, Michelle Guy, and Matthew Perry
United States Geological Survey, Golden, CO 80401, USA

Jan Harms
INFN, Sezione di Firenze, Sesto Fiorentino, 50019, Italy

Nikhil Mukund
*Inter-University Centre for Astronomy and Astrophysics ,
Ganeshkhind, Pune University Campus Pune 411 007, India*

Second-generation ground-based gravitational wave interferometers such as the Laser Interferometer Gravitational-wave Observatory (LIGO) are susceptible to high-amplitude teleseismic events, which can cause astronomical detectors to fall out of mechanical lock (lockloss). This causes the data to be useless for gravitational wave detection around the time of the seismic arrivals and for several hours while the detector stabilizes enough to return to the locked state. The down time can be reduced if advance warning of impending shaking is received and the impact is suppressed in the isolation system with the goal of maintaining lock even at the expense of increased instrumental noise. Here we describe an early warning system for modern gravitational-wave observatories. The system relies on near real-time earthquake alerts provided by the U.S. Geological Survey (USGS) and the National Oceanic and Atmospheric Administration (NOAA). Hypocenter and magnitude information is generally available in 5 to 20 minutes of a significant earthquake. The alerts are used to estimate arrival times and ground velocities at the gravitational wave detectors. In general, 94% of the predictions for ground-motion amplitude are within a factor of 5 of measured values. The error in both arrival time and ground-motion prediction introduced by using preliminary, rather than final, hypocenter and magnitude information is minimal with about 90% of the events falling within a factor of 2 of the final predicted value. By using a Machine Learning Algorithm, we develop a lockloss prediction model that calculates the probability that a given earthquake will prevent a detector from taking data. Our initial results indicate that by using detector control configuration changes, we could save lockloss from 40-100 earthquakes events in a 6-month time-period.

INTRODUCTION

Earthquakes are a significant issue for gravitational-wave detectors. In previous work [1], we described how large-scale astronomical experiments, such as meter class telescopes and gravitational-wave interferometers, are susceptible to earthquakes. In the case of telescopes, the predominant concern was the potential for nearby, devastating earthquakes which will damage either the surrounding structure or the mirrors that make up the telescope. We argued that a regional early earthquake warning (EEW) [2–9] system was important to minimize potential damage to telescopes. Gravitational-wave detectors, on the other hand, are susceptible to teleseismic events from around the world [10]. The Laser Interferometer Gravitational-wave Observatory (LIGO) [11], Virgo [12], and GEO600 [13] detectors are part of a network of gravitational-wave interferometers that have made the first direct observations of gravitational waves [14, 15]. These detectors can be destabilized by significant ground motion, despite seismic isolation systems designed to minimize such effects [16, 17].

During the last LIGO science run, large amplitude earthquakes from around the world would typically cause the detectors to fall out of lock [1]. Not only were the data around the time of the earthquake not useful for gravitational-wave detection, but it would also take hours of dead time for the detectors to return to the locked

state. We showed that there are potential gains to be made with an early warning system assuming that the incurred downtime could be reduced with sufficient advance notice of the earthquakes' arrivals. Detailed studies of earthquake response during S5 and S6 showed that there is about one teleseismic event each week producing ground motion at the sites too strong for the control system to be able to maintain lock. In most cases, it was then impossible to lock the interferometer for some hours. A scheme that would suppress disturbances of earthquakes early in the isolation system with the final goal to maintain lock during strong ground motion, even at the price of increased instrumental noise, could potentially lead to substantial increase of the duty cycle. This will likely be of greater importance even in high-power configurations of the advanced detectors, where thermalization of test masses during the locking procedure could potentially increase the time it takes to reach maximal sensitivity.

For this reason, we have created an earthquake early warning client using a real-time event messaging system of the US Geological Survey. The messages contain information about the fault rupture such as location, depth, magnitude. They are received and processed in real time to estimate arrival times, and seismic amplitudes of the various seismic phases at the detector sites. In addition, it is important to investigate how the client can be implemented. Finally, further effort needs to be spent on investigating the effect of strong ground motion on the aLIGO control system, and to develop methods for adapting the controls as a means of "riding out the earthquake".

In this paper, we will describe seismon , a code developed to mitigate the effects of teleseismic events on ground-based gravitational-wave detectors. It uses event notices received from USGS and makes time of arrival, and amplitude predictions are made for earthquake seismic wave phases at sites of current detectors. Using a combination of earthquake magnitude, distance, and depth information, a prediction of the likelihood of the earthquake causing data disruption at the sites is made.

ALGORITHM

Figure 1 shows the flowchart for the seismon pipeline, developed to mitigate the effects of teleseismic events on ground-based interferometric gravitational wave detectors. It uses event notices received from USGS and makes time of arrival and amplitude predictions for earthquake seismic wave phases at sites of current detectors. Using a combination of earthquake magnitude, distance, and depth information, a prediction of the likelihood of the earthquake causing data disruption at the sites is made.

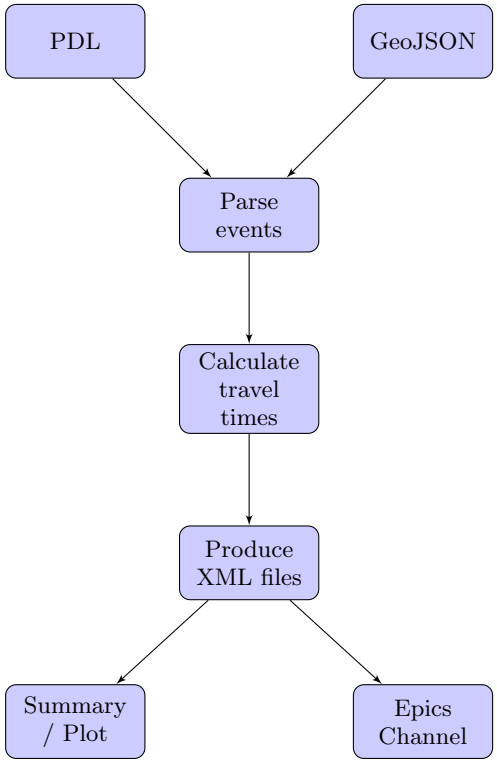

FIG. 1. A flow chart of the seismon pipeline.

Notices

seismon relies on the most preliminary notices of earthquakes currently available generated by worldwide networks of seismometers. In general, the process of identification occurs when a primary or P-wave arrival is identified in a number of nearby seismometers. Preliminary estimates of the location, including latitude, longitude, and depth, are then derived by triangulating these arrivals. Earthquake magnitude estimates, which will also couple into the ground velocity at the gravitational-wave detectors, come later. This is due to the necessity of estimating the distance a fault moved and the force required to move it. Potential warning times becomes a question of how fast P-waves travel relative to secondary or S-waves and surface waves, which travel between 3-6 km/s for S-waves and slightly slower for surface waves. These are more important to gravitational-wave detectors due to their higher amplitude.

The United States Geological Survey (USGS) provides a number of channels for information about earthquakes, on different time-scales. The earliest, which we will use in the pipeline, are automated pipelines which use USGS-supported worldwide networks of seismometers to make earthquake identifications. The earliest solutions provide event source parameters, including both location and magnitude estimates. At later times, seismometer

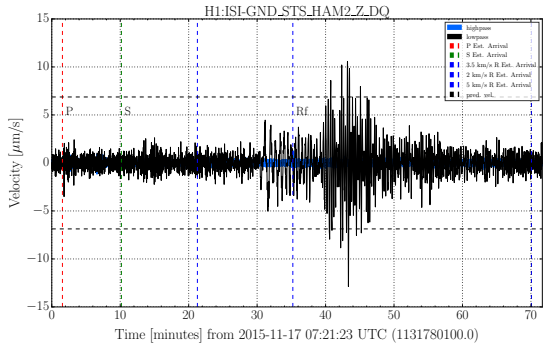

FIG. 2. Time-series of ground motion data from recent earthquake. The plot on the left is the ground motion from a seismometer at the LIGO Hanford site located in Washington, USA for the Nov 17, 2015 6.5 magnitude earthquake in Greece. The P, S, and surface waves all have distinctive arrivals in this case. The surface waves are shown to last tens of minutes.

specific phase, amplitude and magnitude parameters are provided. Furthermore, moment tensor solutions and finite fault models are calculated from the array data. These solutions are distributed through USGS's Product Distribution Layer (PDL), which has been configured to receive all notifications of earthquakes worldwide. As all USGS-supported networks submit notices through this service, the pipeline is ensured to receive all relevant notices. In particular, the notification messages are in the form of either EQXML or QuakeML Extensible Markup Language (XML) files, although the distribution also provides image files and other related content depending on the information. Each network that detects an earthquake provides time-tagged versions of their products, which will allow us to estimate the delay induced by the process of earthquake identification and product distribution. This is a cross-platform Java based code that runs constantly on a dedicated machine.

Analysis

The second step of the process is to convert event notifications to information about the time of arrival and amplitudes at the sites. In summary, we use the location and magnitude estimates the PDL client for two purposes. The first is the time of seismic wave arrivals at the gravitational-wave detectors. The second is the ground motion at the gravitational-wave detectors. Accurate prediction of the ground velocity amplitude based on earthquake magnitude and distance will be required to limit the false alarms. This equation should account for physical effects with variable parameters used to fit to the seismic data currently available. P- and S-wave arrivals can be accurately determined given latitude, longitude, and depth information by calculating travel times using the iaspei-tau package wrapped by Obspy. We can approximate surface waves as having a constant 3.5 km/s speed values.

The second step is to make amplitude predictions for each site. We estimate the peak amplitude of the surface waves, Rf_{amp}, at the sites using equation 1, which we describe below. This was developed as a fit to historical earthquakes at the gravitational-wave detectors. Choosing the peak amplitude was not an arbitrary choice, especially as compared to root-mean-squared (RMS) ground-motion. A RMS value depends on technical calculation choices, which to be effective will depend on the event in question. Eventually it would be appropriate to determine what observational quantity is best suited to predict trouble for the detectors, but for now we adopt peak amplitude due to its relative simplicity. Below, we will show how the inclusion of measured displacement and acceleration, in addition to ground velocity, does not generate significant improvements in lockloss predictability. Both the time-of-arrivals and amplitude prediction are predicted as a function of distance. This allows users of the algorithm to interpolate these metrics for their locations of interest. In general, we generate the predictions for all currently operating gravitational-wave detectors.

We now examine the historical earthquake record and predict the likely ground motion seen. We then use seismic data from on site observations to predict how ground motion will affect the observatories. We have developed an equation attempting to account for physical effects with variable parameters used to fit to the data. Coupling strength of a source at a certain depth to surface Rayleigh waves, dissipation during propagation, geometric amplitude evolution, and frequency dependent scaling of the magnitude into ground displacement were some of the terms used. We estimate the amplitude of the surface waves, Rf_{amp}, at the sites using the equation

$$Rf_{amp} = 10^{-3} M A f e^{-2\pi h f_c/cd} / r^{rs} \quad (1)$$

where $f_c = 10^{2.3-M/2}$, $Af = \frac{Rf_0}{f_c^{Rf_s}}$, M is the magnitude of the earthquake, d is the distance, h is the depth of the earthquake, c is the speed of the surface-waves, and f_c is the corner frequency. These parameters are derived from minimizing the difference between the amplitude seen at the interferometer and that predicted by the equation. To do so, we use a Metropolis Hastings MCMC algorithm implementing adaptive simulated annealing (SA), which statistically guarantees obtaining solutions close to global minima [18, 19]. These are shown for the gravitational-wave detectors in this study in Table . The regression is shown in Fig. 3 for both the LHO and LLO gravitational-wave interferometers. For LHO and LLO, the data was taken from November 2005 to October 2007 (Science Run 5) and July 2009 to October 2010 (Science Run 6). For Virgo, the data was taken

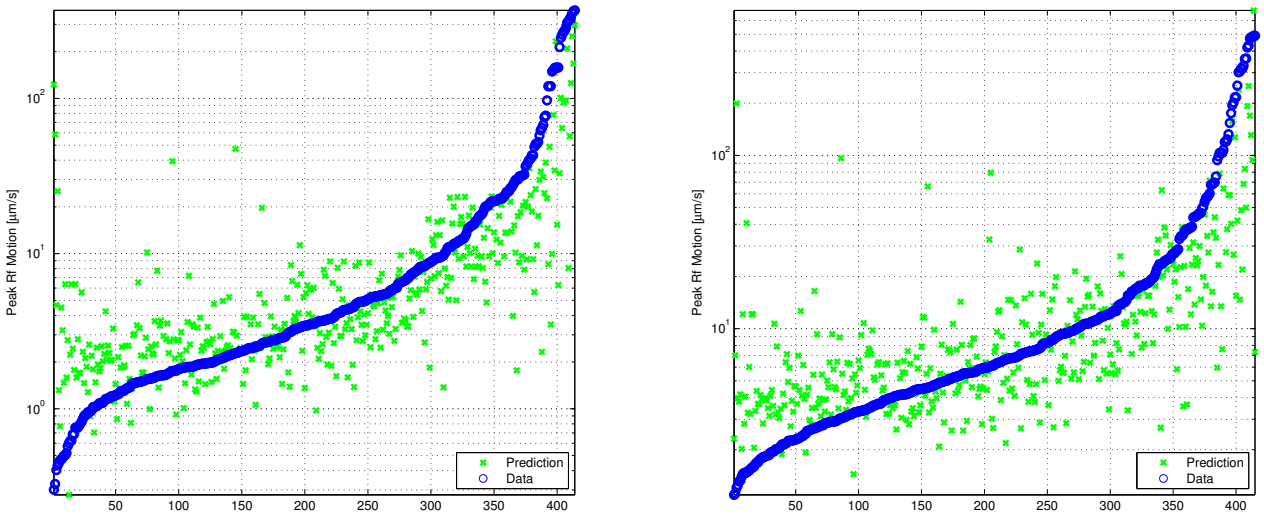

FIG. 3. Fit of peak velocities seen during S5-S6 at the interferometers (LHO and LLO) to equation 1. Fit parameters are estimated from S5-S6 data. The events have been ordered by their measured peak ground velocity (in blue) and the green crosses correspond to the prediction from the equation. About 92% (LHO and LLO) of events are within a factor of 5 of the predicted value.

Detector	Rf_0	Rf_s	cd	rs
LHO	76.44	1.37	440.68	1.57
LLO	0.43	1.40	739.18	0.95
VIRGO	0.21	1.88	497.35	0.86
GEO	4.45	1.14	351.85	1.13

TABLE I. Best fit parameters to the peak velocities seen at the interferometers to equation 1.

from June to September 2011 (Virgo Science Run 4). For GEO, the data was taken from July 2010 to June 2011 (GEO High Frequency). Figure 4 shows the peak ground velocity as a function of magnitude and distance for the models. Based on the above equations, we expect that earthquakes with magnitudes greater than 5 can exceed ground velocities of 1μm/s.

Epics

The final step of the process is to use the site amplitude and time-of-arrival predictions to create warnings (and possibly detector state changes) for the detectors. The algorithm analyzes the recent notifications and places a threshold on the predictions.

We provide an epics variable that contains the following information. The first is the amplitude prediction for any earthquake expected to be present. The second is the probability of lockloss, which is discussed in the next section. The third is when this earthquake is expected to arrive at the site.

PERFORMANCE

In this section, we provide a number of metrics by which we analyze the performance of seismon .

Notification latency

One of the most important qualities of an earthquake monitor is the notification latency, or the amount of warning time a detector has to respond to incoming seismic waves. On the left of figure 5, we show the time delay between the earthquake and generation of the PDL client notification. In general, notices are generated within 5 minutes of the earthquake. On the right of figure 5, the cumulative probability distribution of time delays between the earthquake and approximate arrival of surface waves, assuming surface wave velocities of 3.5 km/s. In general, there is more than 10 minutes available between notification and surface wave arrivals. This is more than sufficient time for gravitational-wave detectors to respond by changing control configurations.

Ground Velocity Prediction Performance

Another important quality for an earthquake monitor is the accuracy of the ground-motion amplitude predic-

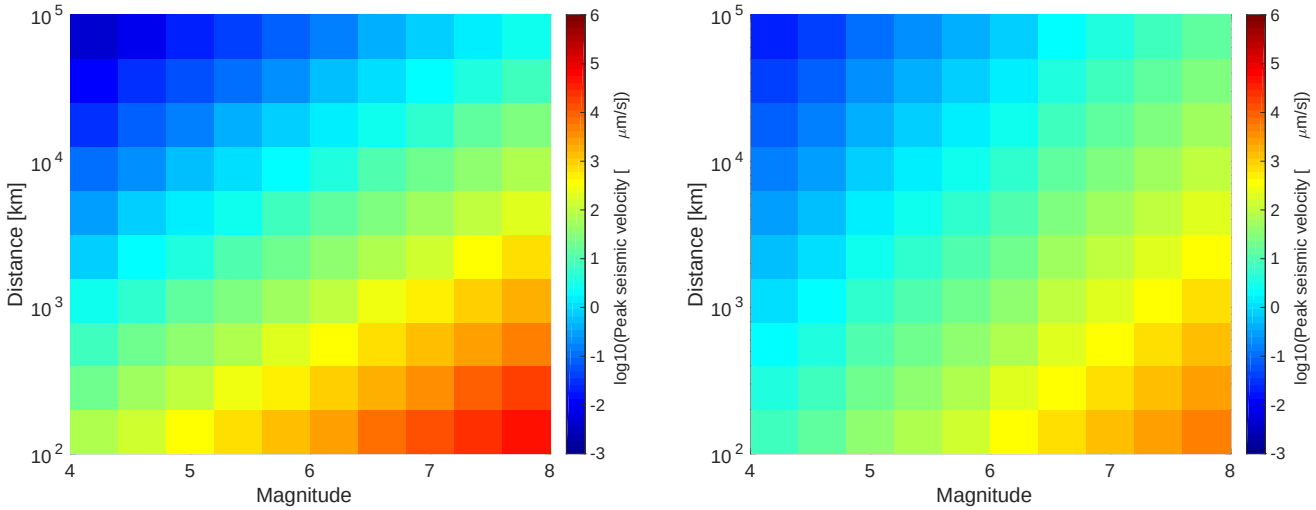

FIG. 4. The predicted peak ground acceleration as a function of magnitude and distance for LHO (left) and LLO (right)

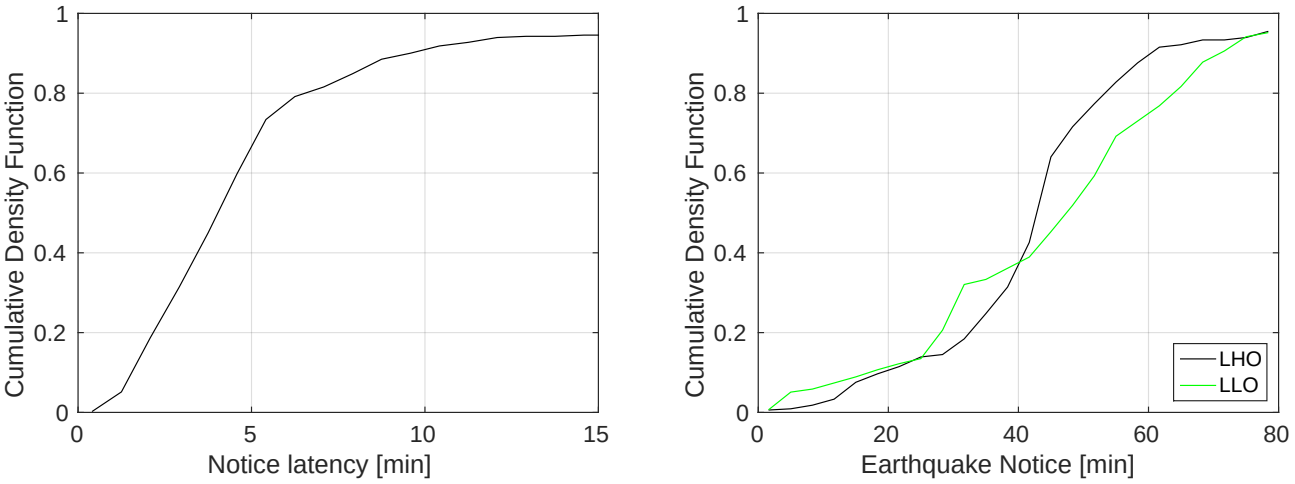

FIG. 5. On the left is the time delay between the earthquake and generation of the PDL client notification. On the right is the time delay between the earthquake notification from the PDL client and approximate arrival of surface waves at the LIGO Hanford site for global earthquakes. A majority of the locations allow for more than a minute of time between notification and site arrival.

tion and the time-of-arrival. The ground-motion amplitude performance is evaluated against the most recent science run (Observing Run 1) from September 2015 to January 2016, in Fig.6. About 94% of events are within a factor of 5, while those that are not are almost exclusively events that are due to the overlap of many events. This occurs often during aftershocks of large earthquakes. As the largest event is the important one, these are unimportant for predictions. There are few events that produce large surface waves without visible body waves. These are more likely to be blasts of some kind. In some cases, there is an under-estimation of the actual seismic speeds. This is likely due to the aliasing due to larger earthquakes, including aftershocks shortly after larger earthquakes.

As mentioned above, seismon uses the earliest available notices for making time-of-arrival and amplitude predictions. Because the earliest notices may only rely on a few seismometers, as well as the fact that large earthquakes do not fault all at once, the estimates for both magnitude, depth, location, and time can be off. In Fig.7, we show the difference of arrival times and predicted peak velocities seen during O1 at the interferometers (LHO and LLO) using the initial and final estimates. About 90% of events are within a factor of 2 of the final predicted value. This is a smaller error than from the regression. In addition, we show the difference between the initial and final estimates of the earthquake time. About 90%

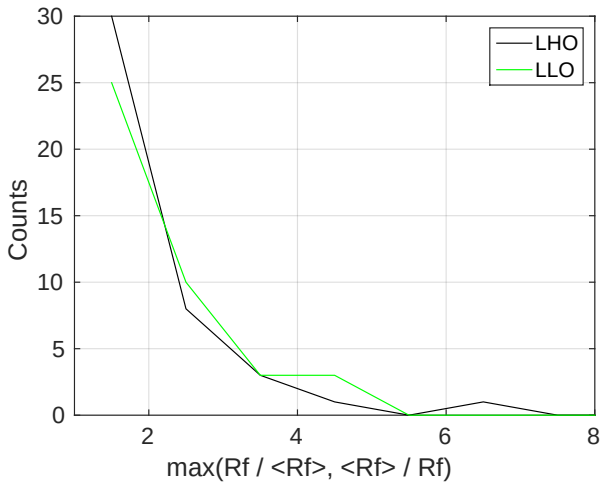

FIG. 6. Performance of estimation of peak velocities seen during O1 at the interferometers (LHO and LLO) using fit parameters estimated from S5-S6 data. About 87% (LHO) and 94% (LLO) of events are within a factor of 5 of the predicted value.

of early estimates are within 3 s of the final time, which is much smaller than the latency from the generation of the notice itself. For these reasons, the use of the early notices is not a major source of systematic error for seismon .

Gravitational-wave detector lockloss prediction performance

An earthquake monitor will only be useful for gravitational-wave detectors if it can be determined which earthquakes cause the loss of data (and which will not affect the detector in a significant way). We now measure the amplitude of the seismic ground motion that causes the detector to lose lock. To do so, we take all known earthquakes above magnitude 5.0 and compute their arrival times. We also determine the times that the gravitational-wave detectors fell out of lock during these times. We then compare these two figures of merit. Fig. 8 shows these times, both for those times when lock losses occurred (red), when they did not (green), and when the detector was not locked (blue). In general, the plot shows that while in general ground velocities greater than about 5 μm/s lead to lock loss, the situation is complicated at lower ground velocities. This motivates using more than ground velocity to predict lockloss.

It is of significant interest to determine the earthquake parameters (and the ground velocities they create) that cause the detectors to lose lock. Given that seismon is an early warning system, the only parameters available for use are those returned by USGS in low latency, which are magnitude, depth and location (and thus distance). In addition, we can use the predicted ground velocity derived from these parameters. The goal is to predict the outcome of the interferometer lock status based on these parameters.

In the following, we will use a Machine Learning Algorithm (MLA) to develop a lockloss prediction model. MLAs, which are useful for classifying and predicting outcomes for various data analysis problems, have been used in the past with great success in gravitational-wave data analysis [20, 21]. We first compare the performance of different machine learning algorithms aimed at modelling lockloss prediction from the given input parameters. All three classifiers : Logistic Regression[22], Naive Bayes[23], Support Vector Machine[24] yield comparable performance with logistic regression giving the best result as is evident from the receiver operator characteristic (ROC) curve shown in Figure 9. Classifier with maximal the area under curve is usually chosen over the others. True positive rate (TPR) is the ratio of sum of predicted positive condition actually being true to the sum of all actually positive conditions. Similarly false positive rate (FPR) is the ratio of sum of predicted positive condition being false to the sum of all actually negative conditions. Positive condition here refers to a lockloss prediction by the classifier which in general can be true or false. Classifier prediction about the detector being in lock forms the negative condition. Threshold value on classifier output (usually a scaled number between 0 and 1 with value close to unity indicative of lockloss) is varied to generate the ROC curve. Seismon makes lockless predictions using the threshold value obtained from optimal operating point of the ROC curve.

We briefly describe how logistic regression can be used to weigh the input parameters to predict the lock status. As lockloss is the only output parameter, this is a single-class classification problem. In this particular analysis, we seek to determine the array θ such that

$$h_\theta = \theta x \tag{2}$$

where h is the lockloss parameter (1 for lockloss, 0 for locked) and x is an array of numerical values corresponding to the input parameters (magnitude, depth, distance, predicted ground velocity). We use a hypothesis function $h = \frac{1}{(1+\theta^T * x)}$ to minimize the difference between the observed and predicted lockloss values. This optimization results in a *theta* array, giving a weight to each parameter in x. These are shown for the gravitational-wave detectors in this study in Table .

To classify the performance of the function, we use plots of real outcomes vs. false alarm probability (FAP). The idea is that by setting the false alarm rate to a certain threshold, we can find a optimum point of efficiency for predicting the outcome. In the analysis that follows, we use $\frac{2}{3}$ of the earthquakes for training and $\frac{1}{3}$ of the earthquakes for the testing set. The *theta* array computed from the training set is applied in the hypothesis

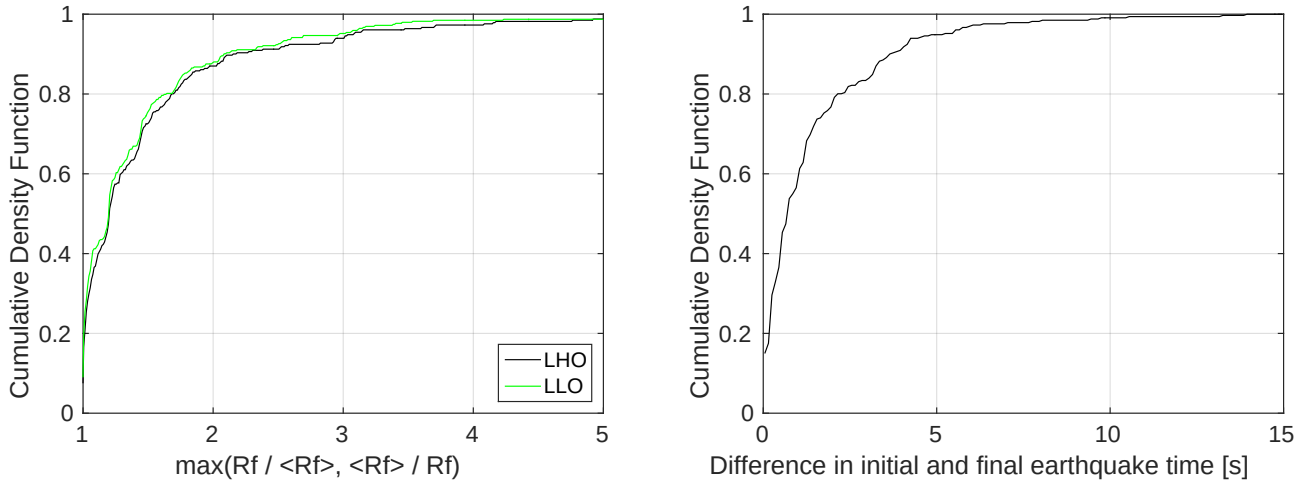

FIG. 7. On the left is the difference of predicted peak velocities seen during O1 at the interferometers (LHO and LLO) using the initial and final estimates. About 90% of events are within a factor of 2 of the final predicted value. On the right is the difference between the initial and final estimates of the earthquake time. About 90% of early estimates are within 4 s of the final time.

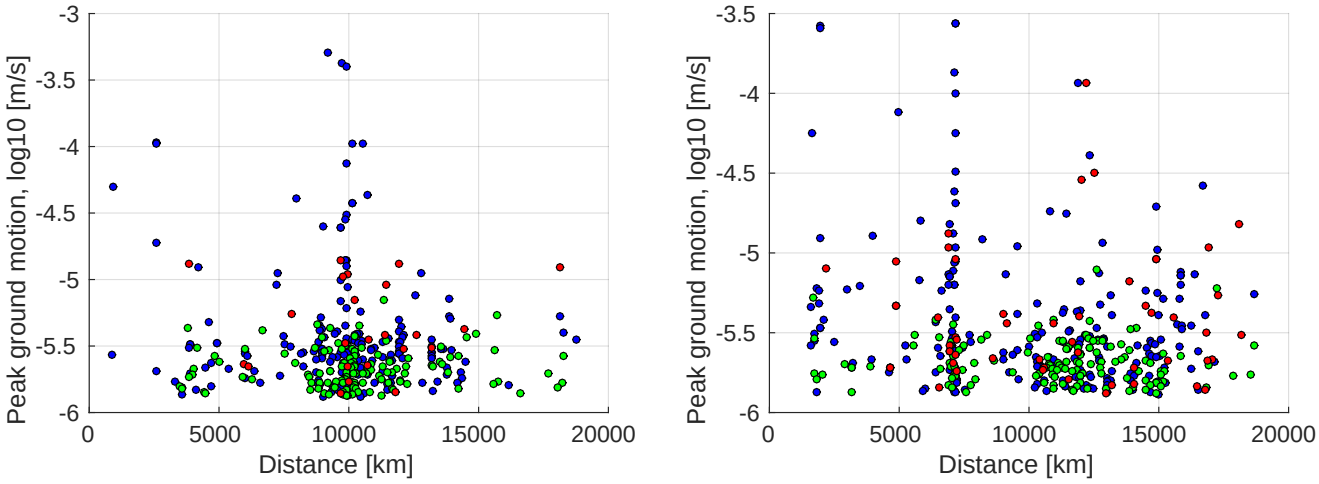

FIG. 8. Lock loss as a function of predicted peak velocity vs. earthquake distance for the gravitational-wave detectors.

Detector	K	M	r	h	Rf
LHO (USGS only)	-6.8	0.06	2.5×10^{-7}	2.1×10^{-3}	1.2×10^{6}
LHO	-24.1	3.4	2.9×10^{-8}	2.7×10^{-3}	9.2×10^{5}
LLO (USGS only)	-6.6	0.28	2.8×10^{-7}	-1.5×10^{-3}	9.6×10^{5}
LLO	-15.3	2.2	5.6×10^{-8}	-1.2×10^{-3}	4.2×10^{5}

TABLE II. Best fit parameters to the θ coefficients from equation 2.

function h_θ for each earthquake in the testing set to determine the predicted outcome of lockstatus. The predicted value for lockloss is determined by rounding the predicted value, which is between 0 and 1, up or down to 1 and 0 respectively.

Figure 10 shows the efficiency curves using the earthquake parameter derived parameters. The curves which include the observed ground velocity at the sites are similar. In general, there is a tradeoff between false alarm probability and efficiency standard probability. The more false alarms one is willing to accept, the higher the rate of earthquakes that will result in lockloss is possible. For example, if we adopt a false alarm probability threshold of 0.5, between 90-100% of earthquakes can be caught.

CONCLUSION

In this paper, we have discussed the problem of earthquakes for gravitational-wave detectors and a pipeline

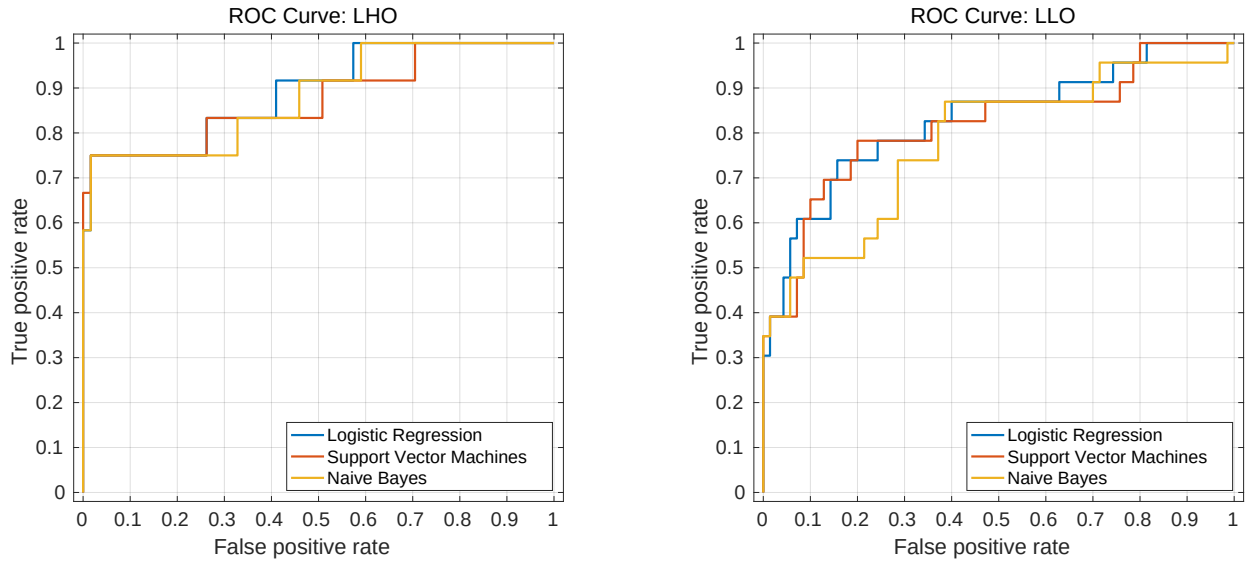

FIG. 9. Performance comparison of different machine learning classifiers

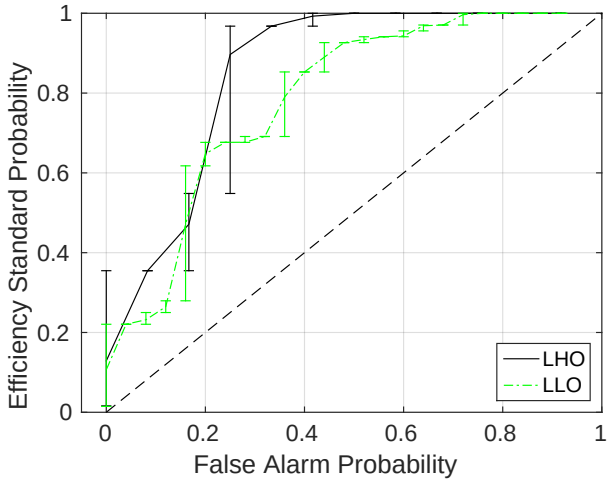

FIG. 10. Efficiency curves using both earthquake parameter derived parameters only as well as one which includes observed ground velocity at the sites.

designed to minimize their impact. We characterize this pipeline in terms of the warning time for these experiments. We have shown that the earthquake warning system can both predict likely earthquake arrival times and ground velocity amplitudes.

A code that performs these steps is available at https://github.com/ligovirgo/seismon/ for public download. Hopefully, this will allow other researchers to easily use the fits. Required inputs are the latitude and longitude of the site and magnitude, latitude, longitude and depth of the source.

In the future, this algorithm will be applied to the next science run. It will require coordination between the low-latency notification software and the detector control systems to maximize the utility of the system. This will include studies of the control configuration best for riding out times of large ground motion.

ACKNOWLEDGMENTS

MC was supported by the National Science Foundation Graduate Research Fellowship Program, under NSF grant number DGE 1144152. NM acknowledges Council for Scientific and Industrial Research (CSIR), India for providing financial support as Senior Research Fellow. LIGO was constructed by the California Institute of Technology and Massachusetts Institute of Technology with funding from the National Science Foundation and operates under cooperative agreement PHY-0757058. This paper has been assigned LIGO document number LIGO-??????????.

[1] Michael Coughlin, Christopher Stubbs, Sergio Barrientos, Chuck Claver, Jan Harms, R. Chris Smith, and Michael Warner. Real-time earthquake warning for astronomical observatories. *Experimental Astronomy*, 39(2):387–404, 2015.

[2] RM. Allen. Transforming earthquake detection? *Science*, 335:297–298, 2012.

[3] Kuyuk, H.S. and RM. Allen. A global approach to provide magnitude estimates for earthquake early warning. *Geophysical Research Letters*, 40, 2013.

[4] Kuyuk, H.S. and RM. Allen. Optimal seismic network density for earthquake early warning: A case study from california. *Seismological Research Letters*, 84(6):946–954, 2013.

[5] Kuyuk, H.S. et al. Designing a network-based earthquake early warning system for california: Elarms-2. *Bulletin of Seismological Society of America*, 104(1), 2014.

[6] Cochran E., Lawrence J., Christensen C., and Chung A. A novel strong-motion seismic network for community participation in earthquake monitoring. *IEEE Inst and Meas*, 12(6):8–15, 2009.

[7] Cochran E., Lawrence J., Christensen C., and Jakka R. The quake-catcher network: Citizen science expanding seismic horizons. *Seismological Research Letters*, 80:26–30, 2009.

[8] M. Bose, R. Allen, H. Brown, G. Gua, M. Fischer, E. Hauksson, T. Heaten, M. Hellweg, M. Liukis, D. Neuhauser, P. Maechling, K. Solanki, M. Vinci, I. Henson, O. Khainovski, S. Kuyuk, M. Carpio, M.-A. Meier, and T. Jordan. Cisn shakealert: An earthquake early warning demonstration system for california. In Friedemann Wenzel and Jochen Zschau, editors, *Early Warning for Geological Disasters*, Advanced Technologies in Earth Sciences, pages 49–69. Springer Berlin Heidelberg, 2014.

[9] Mitsuyuki Hoshiba, Osamu Kamigaichi, Makoto Saito, Shin'ya Tsukada, and Nobuo Hamada. Earthquake early warning starts nationwide in japan. *Eos, Transactions American Geophysical Union*, 89(8):73–74, 2008.

[10] D M Macleod, S Fairhurst, B Hughey, A P Lundgren, L Pekowsky, J Rollins, and J R Smith. Reducing the effect of seismic noise in ligo searches by targeted veto generation. *Classical and Quantum Gravity*, 29(5):055006, 2012.

[11] J Aasi et al. Advanced ligo. *Classical and Quantum Gravity*, 32(7):074001, 2015.

[12] F Acernese et al. Advanced virgo: a second-generation interferometric gravitational wave detector. *Classical and Quantum Gravity*, 32(2):024001, 2015.

[13] Grote H. for the LIGO Scientific Collaboration. The GEO 600 status. *Class. Quantum Grav.*, 27:084003, 2010.

[14] Abbott, B. P. et al. Observation of gravitational waves from a binary black hole merger. *Phys. Rev. Lett.*, 116:061102, Feb 2016.

[15] Abbott, B. P. et al. Gw151226: Observation of gravitational waves from a 22-solar-mass binary black hole coalescence. *Phys. Rev. Lett.*, 116:241103, Jun 2016.

[16] R Abbott, R Adhikari, et al. Seismic isolation for advanced ligo. *Classical and Quantum Gravity*, 19(7):1591, 2002.

[17] Alberto Stochino, Benjamin Abbot, Yoichi Aso, Mark Barton, Alessandro Bertolini, Valerio Boschi, Dennis Coyne, Riccardo DeSalvo, Carlo Galli, Yumei Huang, Alex Ivanov, Szabolcs Marka, David Ottaway, Virginio Sannibale, Chiara Vanni, Hiroaki Yamamoto, and Sanichiro Yoshida. The seismic attenuation system (sas) for the advanced LIGO gravitational wave interferometric detectors. *Nuclear Instruments and Methods in Physics Research Section A: Accelerators, Spectrometers, Detectors and Associated Equipment*, 598(3):737 – 753, 2009.

[18] S. Kirkpatrick, C. D. Gelatt, and M. P. Vecchi. Optimization by simulated annealing. *Science*, 220(4598):671–680, 1983.

[19] Lester Ingber. Adaptive simulated annealing (ASA): lessons learned. *CoRR*, cs.MS/0001018, 2000.

[20] Rahul Biswas, Lindy Blackburn, Junwei Cao, Reed Essick, Kari Alison Hodge, Erotokritos Katsavounidis, Kyungmin Kim, Young-Min Kim, Eric-Olivier Le Bigot, Chang-Hwan Lee, John J. Oh, Sang Hoon Oh, Edwin J. Son, Ye Tao, Ruslan Vaulin, and Xiaoge Wang. Application of machine learning algorithms to the study of noise artifacts in gravitational-wave data. *Phys. Rev. D*, 88:062003, Sep 2013.

[21] Kyungmin Kim, Ian W Harry, Kari A Hodge, Young-Min Kim, Chang-Hwan Lee, Hyun Kyu Lee, John J Oh, Sang Hoon Oh, and Edwin J Son. Application of artificial neural network to search for gravitational-wave signals associated with short gamma-ray bursts. *Classical and Quantum Gravity*, 32(24):245002, 2015.

[22] Peter McCullagh and John A Nelder. *Generalized linear models*, volume 37. CRC press, 1989.

[23] George H. John and Pat Langley. Estimating continuous distributions in bayesian classifiers. In *Proceedings of the Eleventh Conference on Uncertainty in Artificial Intelligence*, UAI'95, pages 338–345, San Francisco, CA, USA, 1995. Morgan Kaufmann Publishers Inc.

[24] Christopher J. C. Burges. A tutorial on support vector machines for pattern recognition. *Data Min. Knowl. Discov.*, 2(2):121–167, June 1998.